

Analyzing Machupo virus-receptor binding by molecular dynamics simulations

Austin G. Meyer^{1,2,3*}, Sara L. Sawyer², Andrew D. Ellington²,
and Claus O. Wilke¹

Address:

¹Department of Integrative Biology, Institute for Cellular and Molecular Biology, and Center for Computational Biology and Bioinformatics. The University of Texas at Austin, Austin, TX 78712, USA.

²Department of Molecular Biosciences, Institute for Cellular and Molecular Biology, The University of Texas at Austin, Austin, TX 78712, USA.

³School of Medicine, Texas Tech University Health Sciences Center, Lubbock, TX 79430, USA.

*Corresponding author

Email: austin.meyer@utexas.edu

Phone: +1 512 971 0123

Manuscript type: research article

Keywords: protein–protein interaction, molecular dynamics, arenavirus, machupo

Abstract

1
2 In many biological applications, we would like to be able to computationally predict muta-
3 tional effects on affinity in protein-protein interactions. However, many commonly used meth-
4 ods to predict these effects perform poorly in important test cases. In particular, the effects
5 of multiple mutations, nonalanine substitutions, and flexible loops are difficult to predict with
6 available tools and protocols. We present here an existing method applied in a novel way to
7 a new test case; we interrogate affinity differences resulting from mutations in a host-virus
8 protein-protein interface. We use steered molecular dynamics (SMD) to computationally pull
9 the machupo virus (MACV) spike glycoprotein (GP1) away from the human transferrin recep-
10 tor (hTfR1). We then approximate affinity using the maximum applied force of separation and
11 the area under the force-versus-distance curve. We find, even without the rigor and planning
12 required for free energy calculations, that these quantities can provide novel biophysical insight
13 into the GP1/hTfR1 interaction. First, with no prior knowledge of the system we can differenti-
14 ate among wild type and mutant complexes. Moreover, we show that this simple SMD scheme
15 correlates well with relative free energy differences computed via free energy perturbation.
16 Second, although the static co-crystal structure shows two large hydrogen-bonding networks in
17 the GP1/hTfR1 interface, our simulations indicate that one of them may not be important for
18 tight binding. Third, one viral site known to be critical for infection may mark an important
19 evolutionary suppressor site for infection-resistant hTfR1 mutants. Finally, our approach pro-
20 vides a framework to compare the effects of multiple mutations, individually and jointly, on
21 protein protein interactions.

22 **1 Introduction**

23 The computational prediction of mutational effects on protein–protein interactions remains a chal-
24 lenging problem. Several methods are available to perform an energy difference calculation from an
25 experimentally determined co-crystal structure. For example, end point methods can be performed
26 rapidly, with relatively low computational cost (Gront et al. 2011; Kortemme et al. 2004). How-
27 ever, such methods can suffer from various simplifying assumptions. For example, they generally
28 use an implicit solvent approximation and assume the end state difference with minimal structural
29 rearrangement is sufficient to discriminate energetic differences (Gront et al. 2011; Kortemme et al.
30 2004). Alternative approaches have been developed using machine learning, training coefficients
31 in a weighted equation containing geometric and energetic parameters (Vreven et al. 2011, 2012;
32 Bajaj et al. 2011; Hwang et al. 2010). Unfortunately, such machine-learning approaches often suf-
33 fer in novel applications, for which available training sets are small or non-existent. As such, these
34 methods are poorly suited for most host-virus protein–protein systems. By contrast, first principles
35 methods can forgo training, but currently available methods such as free energy perturbation (FEP)
36 and thermodynamic integration (TI) rely on a transitional model (where one state may be wild-type
37 and the other may be a mutant) to make rigorous free energy calculations (Gilson et al. 1997; Lu
38 et al. 2004; Chodera et al. 2011; Gumbart et al. 2013a). While these may be considered two of the
39 gold standard techniques for calculating affinity differences, there are a huge number of theoret-
40 ical and technical complexities that must all be properly managed to ensure a converged solution
41 (Gumbart et al. 2013b). Such considerations quickly come to dominate the protocol, and the nec-
42 essary book keeping introduces the possibility of human error (Gumbart et al. 2013b). Moreover,
43 as the two ending states look ever more dissimilar the chances of convergence fall rapidly. To en-
44 sure convergence, these techniques are typically limited to small differences (such as point mutant
45 comparisons) with a few, very impressive exceptions (Wang et al. 2006; Gumbart et al. 2013a,b).
46 For most investigators, larger differences quickly become intractable as the number of intermedi-
47 ate steps required to compute a converged solution grows or the complexity of adding restraining
48 potentials and computing approximations expands (Wang et al. 2006; Gumbart et al. 2013a,b).

49 Here we propose that much of these complexities can be avoided if all we are interested in is a
50 relative comparison of the effects of different mutations on protein-protein interactions, rather than

51 measuring an absolute or relative binding affinity with experimentally realistic units. We impart
52 a pulling force within an all-atom molecular dynamics simulation on one member of the complex
53 while the other is held in place. Then, we measure the force required for dissociation (Lu and
54 Schulten 1999; Isralewitz et al. 2001b,a; Park and Schulten 2004; Gumbart et al. 2012; Miño et al.
55 2013). Although such biasing techniques are commonly used in protein-ligand binding problems,
56 they are less commonly applied to protein-protein interactions, and almost never to mutational
57 analysis in a protein-protein system. This is largely the result of free energy convergence dif-
58 ficulties and computational limitations (Cuendet and Michielin 2008; Cuendet and Zoete 2011).
59 Using a proxy for relative binding affinity rather than calculating absolute affinities can solve these
60 problems. Here, as proxies, we use the maximum applied force required for separation and the
61 area under the force-versus-distance curve (AUC). For comparison, we also calculate relative free
62 energy differences using the traditional dual topology FEP paradigm, and we show that the two
63 approaches yield congruent results.

64 We used SMD and FEP to interrogate the interaction between machupo virus (MACV) spike
65 glycoprotein (GP1) and the human transferrin receptor (hTfR1) (Abraham et al. 2010; Charrel and
66 de Lamballerie 2003). Machupo virus is an ambisense RNA virus of the arenavirus family (Char-
67 rel and de Lamballerie 2003). Worldwide, arenaviruses represent a significant source of emerging
68 zoonotic diseases for the human population (Charrel and de Lamballerie 2003). Members of the
69 arenavirus family include the Lassa fever virus endemic to West Africa, the lymphochoriomenin-
70 gitis virus (LCMV) endemic to rodents in several areas of the United States, and the Guanarito,
71 Junin, and Machupo viruses endemic to rodents in South America (Charrel and de Lamballerie
72 2003). The South American arenaviruses typically infect humans after rodent contamination and
73 can cause a devastating hemorrhagic fever with high mortality (Charrel and de Lamballerie 2003).

74 The hTfR1 is the primary receptor used by MACV for binding its host cell prior to infection.
75 The primary role of hTfR1 *in vivo* is to bind transferrin for cellular iron uptake. The hTfR1 protein
76 contains three extracellular domains: two basilar domains and an apical domain. The two basilar
77 domains serve most of the transferrin-binding function (Abraham et al. 2010; Radoshitsky et al.
78 2011). Viral entry is initiated by GP1 binding to the apical domain of hTfR1. Previous work has
79 indicated that the GP1/hTfR1 binding interaction is the primary determinant of MACV host range
80 variation (Choe et al. 2011; Radoshitsky et al. 2011). The co-crystal structure shows that the high

81 affinity interaction between GP1 and hTfR1 forces the normally flexible loop in the apical domain
82 of hTfR1 into a rigid β -pleated sheet domain. For GP1, several extended loops mediate binding to
83 hTfR1 (Abraham et al. 2010; Radoshitsky et al. 2011), and many of the interface interactions are
84 mediated by extensive hydrogen-bonding networks (Abraham et al. 2010). Experimental alanine-
85 scanning and whole-cell infectivity assays have identified several sites in both GP1 and hTfR1 that
86 are probably critical for establishing infection (Choe et al. 2011; Radoshitsky et al. 2011).

87 We applied our computational method to wild type (WT) and mutant complexes, and found
88 that we could resolve relative differences in unbinding and predict significant affinity changes.
89 Importantly, the affinity changes predicted using only max force or AUC show a strong correlation
90 with rigorous relative free energy differences computed by FEP. At sites known to be important for
91 successful viral entry, we found that the biochemical cause of reduced infectivity may not be as
92 simple as the static structure suggests. For example, the static structure shows a hydrogen-bonding
93 network connected to site Asn348 in hTfR1. According to our simulations, this network may not
94 affect binding affinity directly. In addition, our study offers an all-atom steered molecular dynamic
95 approach to avoid some of the pitfalls of several existing methods used to evaluate mutations in
96 protein–protein interfaces.

97 **2 Materials and Methods**

98 **2.1 System Modeling**

99 For our experiments, we used the experimentally determined GP1/hTfR1 structure (PDB-ID: 3KAS)
100 (Abraham et al. 2010). The apical domain of hTfR1 interacts directly with GP1 while the other two
101 domains are closer to the cell membrane and have essentially no interaction with GP1. The bio-
102 physical independence of the apical domain allowed us to isolate it without significantly affecting
103 the GP1/hTfR1 interaction.

104 We used the protein visualization software PyMOL (Schrödinger 2010) to remove residues
105 121-190, 301-329, and 383-756 in the hTfR1. No residues were removed from the viral protein.
106 Figure 1 shows a model of the initial structure and that of the pared structure. Although GP1 has
107 several glycosylatable residues, we opted to use the de-glycosylated protein for this study. The

108 complexity of correctly parameterizing diverse sugar moieties is outside of the scope of this paper.
109 Furthermore, although it is known that GPI is glycosylated, and some of those sugars contact
110 hTfR1, the sugars in the available PDB structure are not physiological for mammals (Abraham
111 et al. 2010). In total we removed 10 sugars from the crystal structure for this study.

112 After system reduction, the Visual Molecular Dynamics (VMD) (Humphrey et al. 1996) pack-
113 age along with its system of back-ends was used for all subsequent modeling. The Orient add-on
114 package allowed us to rotate the system axis such that the direction of steering was oriented di-
115 rectly down the z-axis. De-glycosylation simplified the system such that Autopsf could easily find
116 the chain terminations and patch them appropriately. The Solvate package was used to generate a
117 TIP3P water model with a 5 Ångstrom buffer (relative to the maximum dimensions of the proteins)
118 on all sides except down the positive z-axis where a 20 Ångstrom buffer was created. Finally, we
119 used the Autoionize package to place 150 millimolar NaCl and neutralize the total system charge.
120 In the end, each modeled system had approximately 28,000 atoms.

121 **2.2 Equilibration**

122 NAMD was used for all simulations in this study (Phillips et al. 2005). In addition to the modeled
123 system, for equilibration we generated a configuration file that fixed the α -carbon backbone. This
124 was accomplished by setting the B-factor column to 1 for the fixed atoms and to zero for all other
125 atoms. Further, we generated a configuration file with fixed α -carbon atoms at residues 41-92 (num-
126 bered linearly, in this case, starting at 1 for the first amino acid as was required for NAMD) in the
127 hTfR1. The second file was used to affix a harmonic restraint, thus preventing any unfolding due to
128 system reduction. More importantly, the harmonic restraint allowed the protein complex to equili-
129 brate while preventing any drift from its predefined position; the restraint did not constrain the struc-
130 ture of each protein, or the relative position or orientation of the two proteins to each other. Finally,
131 we calculated the system center and dimensions for use in molecular dynamics settings. The exact
132 NAMD configuration files are available on github (https://github.com/clauswilke/MACV_SMD).

133 We used the Charmm27 (Brooks et al. 1983) all-atom force field. The initial system temperature
134 was set to 310K. Several typical MD settings were used including switching and cutoff distances
135 (see provided configuration files). In addition, we used a 2 femtosecond time step with rigid bonds.
136 We used periodic boundary conditions with the particle mesh ewald (PME) method of computing

137 full system electrostatics outside of the explicit box. Furthermore, we used a group pressure cell,
138 flexible box, langevin barostat, and langevin thermostat during equilibration. A harmonic restraint
139 (called harmonic constraint in VMD) was set as stated previously.

140 To start the simulation, the barostat was switched off and the system was minimized for 1000
141 steps. Next, the fixed backbone was released, and the system was minimized for an additional 1000
142 time steps. Subsequently, the system was released into all-atom molecular dynamics for 3000 steps.
143 Finally, the langevin barostat was turned on and the system was simulated for 2 ns (1,000,000 steps)
144 of chemical time. For each mutant, twenty independent equilibration replicates were run with an
145 identical protocol.

146 **2.3 Steered Molecular Dynamics**

147 We used the final state from each equilibrated system to restart another MD simulation. Our steer-
148 ing protocol is fundamentally similar to Cuendet and Michielin (2008) with slightly different pa-
149 rameter choices. Perhaps the one significant difference lies in our choosing to not use a thermostat
150 or barostat. We can make this choice because we are not trying to calculate the binding free en-
151 ergy by any physically rigorous approach (the Jarzynski inequality being one example). Following
152 equilibration, the final state of each simulation was used to generate a configuration file fixing the
153 α -carbon on residues 1, 58, 73-83, 96, 136, 137, 138, and 161 (again with linear numbering) in
154 the hTfR1. These residues were selected as they are far from the binding interface and sufficiently
155 distributed to prevent any orientational motion of the receptor relative to the viral spike protein.
156 The center of mass of the α -carbons of all residues (163-318 in linear numbering) in GP1 received
157 an applied force during the simulation. The NAMD convention does not actually apply a force to
158 all α -carbon atoms but rather uses the selection to compute an initial center of mass. Then, during
159 the steering run, the single center of mass point is pulled with the parameters described below.
160 We used the same force field parameters (exclude, cutoff, switching, etc.), the same integrator pa-
161 rameters (time step, rigidbonds on, all molecular being wrapped, etc.), and the same particle mesh
162 ewald parameters as in equilibration. Periodic boundary conditions were incorporated as part of
163 the system (as is the convention in NAMD restart) and PME was again used to approximate full
164 system electrostatics.

165 We ran test simulations at several force constants and visually inspected the results. A force

166 constant of 5 kcal/mol/Å² was chosen due to its relatively low signal-to-noise ratio. This constant
167 is slightly lower than the more common 7 kcal/mol/Å² found in several recent studies; that value is
168 commonly selected primarily because it is the force constant found in the SMD tutorial available
169 through the NAMD developers. Moreover, the force constant could very likely be set to a range of
170 nearby values with little loss in predictive power.

171 In SMD experiments the pulling velocity should be as low as possible for the available com-
172 putational time (Cuendet and Michielin 2008; Cuendet and Zoete 2011). We choose a velocity of
173 0.000001 Å/fs = 1 Å/ns, and direction down the positive z -axis. One could use faster pulling if
174 the computing time must be reduced, but slower than necessary pulling speeds are not typically
175 considered problematic.

176 SMD was run for 15 ns (7,500,000 time steps) of chemical time. For each simulation, we
177 randomly selected one of the equilibration runs for restart. We ran 50 replicate simulations per
178 mutant for a total of 550 SMD simulations. All GP1/hTfR1 complexes separated by greater than 4
179 Å and many separated to 10 or more.

180 To leave the final trajectory of a tractable size, only 1000 evenly spaced frames were retained
181 from each simulation, leaving a final trajectory size of 323 MB. See the supplemental movie for
182 a representative unbinding trajectory. Initial development of the SMD protocol was carried out
183 on the Lonestar cluster at the Texas Advanced Computing Center (TACC). All production SMD
184 simulations were performed on the Hrothgar cluster at Texas Tech University, using NAMD 2.9.
185 Each simulation was parallelized over 60 computational cores and utilized approximately 20 hours
186 of computing time. The total chemical time simulated for this project was nearly 10 μ s, requiring
187 slightly over 1 million cpu-hours.

188 **2.4 Free Energy Perturbation**

189 Briefly, we used the traditional dual topology approach to FEP (Gao et al. 1989; Pearlman 1989).
190 This involves a thermodynamic cycle where a set of atoms are progressively decoupled from the
191 environment while another set of atoms are progressively coupled. To compute the relative free
192 energy difference requires knowing the free energy change when the transformation is carried out
193 for the bound complex and the individual protein. Then, one can compute the relative free energy
194 difference between a WT and mutant complex by taking the difference between the energy required

195 to decouple/couple the atoms in solution from the energy required to decouple/couple the atoms in
196 the bound complex (Gao et al. 1989; Pearlman 1989).

197 Again, the NAMD configuration file is made available via github (https://github.com/clauswilke/MACV_SMD)
198 We used a similar configuration to that in equilibration. One significant difference was to make a
199 cubic water box with a side length equal to the long axis of the complex plus a 10 Å buffer on either
200 side, and simply restrict center of mass motion with the NAMD setting. This was done to avoid
201 affecting the system energy while calculating free energy differences.

202 The transition protocol for bound and free protein systems were identical. They started with
203 1000 steps of minimization and 250,000 steps of equilibration in the starting state for the forward
204 and reverse directions. Phase transitions were carried out in steps of $\lambda=0.05$. Each transition
205 was carried out for 250,000 steps. The first 100,000 steps after phase transition were reserved for
206 equilibration and the final 150,000 steps were used for data collection.

207 The VMD mutator tool was used to generate the necessary topology file and the parseFEP tool
208 (Liu et al. 2012) in VMD was used for subsequent analysis. We used it to perform error analysis
209 and compute the Bennett acceptance ratio as the maximum likelihood free energy difference of the
210 two states under consideration. Though the larger transitions presented difficulty in a small number
211 of windows, forward and reverse hysteresis was generally in good agreement for all complexes.
212 The double mutants were performed by first doing the Y211A mutation followed by the other of
213 the two mutants. Then, the ΔG 's were simply added together to get the total energetic difference.

214 **2.5 Post-processing**

215 The python packages MDAnalysis (Michaud-Agrawal et al. 2011) and ProDy (Bakan et al. 2011)
216 were both used at various points in post-processing. The molecular trajectory (comprising the
217 atomic coordinates per time) was parsed to compute the center-of-mass for each of the two com-
218 plexes. The starting center-of-mass distance was set to zero and the distance was re-computed at
219 each time step relative to the starting distance.

220 The statistical package R was used for all further analysis and visualization. Each of the 50
221 independent trajectories per mutant produced a fairly noisy force curve. The force curves for each
222 mutant were smoothed over all replicates by using the `smooth.spline()` and `predict()` functions in R
223 with default settings. The two primary descriptive statistics we used were maximum interpolated

224 applied force and total area under the interpolated curve (AUC). We tested for significant differences
225 in maximum force or AUC by carrying out t tests for all pairwise combinations (each mutant com-
226 pared to each other mutant), using the `pairwise.t.test()` function in R. We adjusted p values to cor-
227 rect for multiple testing using the False-Discovery-Rate (FDR) method (Benjamini and Hochberg
228 1995). The `ggplot` (Wickham 2009) package was used to generate most of the figures.

229 Analysis scripts and final data (except MD trajectories) are available on the github repository
230 accompanying this publication (https://github.com/clauswilke/MACV_SMD).

231 **3 Results**

232 **3.1 The GP1/hTfR1 system**

233 The GP1/hTfR1 interface marks a particularly important and useful test system. There are sev-
234 eral sites on both the human and viral protein known to affect the infectivity phenotype of MACV.
235 Many of the important sites have been mapped by *in vitro* flow-cytometry based entry assays. The
236 GP1/hTfR1 interface appears not to be dominated by one particular type of interaction (electro-
237 statics, hydrogen-bonding, or van der Waals). In addition, much of the binding domain on hTfR1
238 is on a loop that is flexible prior to viral binding, but organizes to become a strand of a β -sheet
239 on binding. As a result, many other computational techniques (Gront et al. 2011; Kortemme et al.
240 2004) are only marginally useful. The complex nature of this interface represents a particularly
241 difficult challenge for traditional computational analysis.

242 In total, we tested 7 point mutants and 3 double mutants in addition to the WT complex (Table 1
243 and Figure 8). All of the mutations are within 5 Å of the protein–protein interface. Mutations in
244 hTfR1 at site 211 have proven capable of causing loss-of-entry according to *in vitro* flow-cytometry
245 infection assays or known host-range limitations (Radoshitsky et al. 2008; Choe et al. 2011; Ra-
246 doshitsky et al. 2011). Most likely, this effect is caused by the destruction of a critical hydrogen
247 bond to Ser113 or Ser111 in GP1. The lost hydrogen bond would lead to the subsequent loss of a
248 large hydrogen-bonding network seen in the crystal structure (Table 1) (Abraham et al. 2010). In a
249 manner similar to site 211, Asn348 appears to be important for binding by participating in a critical
250 hydrogen bonding network (Radoshitsky et al. 2008; Abraham et al. 2010) to GP1. In particular,

251 Asn348Lys is reported in the literature to cause significantly reduced viral entry *in vivo* (Table 1)
252 (Radoshitsky et al. 2008; Abraham et al. 2010). Finally, an alanine mutation at site 111 in GP1
253 (mutation vArg111Ala) has also been shown to cause decreased entry (Table 1) (Radoshitsky et al.
254 2011). For notation purposes, the viral site is always referred to with a preceding ‘v’.

255 Despite the fact that viral binding occurs at the site of a flexible loop in the free hTfR structure,
256 our data shows after binding the strand is extremely rigid. In the bound conformation, only two
257 sites of the loop have root mean squared fluctuation (RMSF) values in the top half of all receptor
258 sites during equilibration (Figure 2), and those are almost completely exposed to solvent. This is
259 unsurprising considering the high degree of burial that occurs as a result of viral binding. Com-
260 puting the root mean squared deviation (RMSD) of the entire structure over the trajectory shows
261 that none of the mutations are so deleterious as to cause rapid unbinding. In fact, the RMSD over
262 trajectory looks highly invariant across mutants (Figure 3). In the unbound state, calculated near
263 the end of the SMD trajectory, all of the residues in the WT receptor interfacial strand are in the
264 top half of RMSF over all receptor sites (Figure 4). Thus, if sufficient simulation time is not ded-
265 icated to allowing this unfolding process, standard free energy techniques may miss the energetic
266 contributions that result from ordering the flexible loop in the hTfR apical domain.

267 **3.2 Molecular dynamics simulations**

268 We analyzed the GP1/hTfR1 system using two molecular dynamics techniques. First, by carrying
269 out SMD using a known force constant and pulling with a constant velocity, we could calculate
270 the applied force during protein–protein dissociation (Cuendet and Michielin 2008; Cuendet and
271 Zoete 2011). A typical averaged force curve comparison can be seen in Figure 5, and individual
272 images of all averaged force curves are available in the associated github repository, in folder
273 figures/force_curves. As seen in Figure 5, the dissociation distance was relatively consistent among
274 mutants. The supplementary movie visually illustrates the separation distance between peptide
275 domains. The quantities maximum applied force and AUC were derived from the force-versus-
276 distances curves. Their summary statistics are reported in Table 2. As we are more interested in
277 the phenotypic impact of interface mutations we avoided many of the more physically rigorous, but
278 technically complicated calculations that are possible with SMD (Isralewitz et al. 2001b,a).

279 Before systematically applying SMD to the GP1/hTfR1 interaction, we needed to ensure the

280 method was sufficiently sensitive to distinguish between relatively minor point mutations. While
281 SMD has been applied previously to measure the binding energy of high-affinity T-cell receptor
282 interactions (Cuendet and Michielin 2008; Cuendet and Zoete 2011), it is rarely used to parse small
283 energy differences in a protein–protein interaction energy landscape. For this initial sensitivity anal-
284 ysis, we tested alanine substitutions congruent with the traditional experimental and computational
285 approach.

286 We proceeded to compare our SMD results to that of the standard dual topology FEP approach
287 to calculate relative free energy differences. The correlation between the energetically rigorous
288 FEP and our statistical approach is high. For all 11 complexes tested, the correlation between max
289 force and FEP was $r = -0.795$ at $p = 0.0034$ (Figure 7), and the correlation between AUC and
290 FEP was $r = -0.593$ at $p = 0.055$. Because of the strong correlation, we refer exclusively to the
291 SMD results for the remainder of this work, focusing primarily on max force.

292 We found that relative to WT, one alanine mutation (Tyr211Ala) produced a very large and
293 statistically significant difference in the maximum applied force and AUC (Figure 5, Table 3),
294 while the other two did not (Table 3). When considering additional mutants (also discussed below),
295 we found that maximum applied force was generally sufficient to distinguish mutants (Tables 3
296 and 4), and AUC was able to add a few more statistically significant differences (Table 5). In
297 general, however, and consistent with the FEP results, maximum applied force seemed to be the
298 more sensitive statistic than AUC.

299 **3.3 Comparative analysis of the GP1/hTfR1 interface**

300 Considering the involvement of extended hydrogen-bonding networks in the GP1/hTfR1 interface,
301 it was not clear that individual alanine mutations, even those that should destroy such networks,
302 would significantly change the strength of interaction. One major advantage of first principles sim-
303 ulations is the ability to test mutations other than alanine without additional underlying assumptions
304 in the energy function. As shown in Table 1, we made additional mutations based on biochemical
305 intuition or available experimental data to chemically diverse amino acids including tryptophan,
306 lysine, aspartate, and threonine. Several mutations caused significant relative affinity changes. In
307 addition, to detect synergistic effects, we tested several double mutants where both mutations ap-
308 peared to cause similar changes in binding. Then, we compared the size of those differences to

309 single mutants (Figure 6 and 8).

310 Although Tyr211Ala appears to have a large impact on binding affinity, no single mutant can
311 provide enough evidence to understand the biochemical difference in binding mechanism. Since
312 alanine is both smaller than tyrosine and also incapable of participating in hydrogen-bond inter-
313 actions, we tested further mutations to identify the critical biochemical difference responsible for
314 change in binding affinity. In particular, we substituted smaller side chains that, like tyrosine, were
315 capable of hydrogen bonding. We chose Tyr211Asp and Tyr211Thr, two mutations that have been
316 discussed in the context of selection pressure on hosts in rodent populations (Radoshitsky et al.
317 2008; Choe et al. 2011; Radoshitsky et al. 2011). Both mutations proved capable of causing a
318 significant change in binding affinity in our simulations, but the change appeared to be increased
319 affinity (Figures 6 and 8, and Table 4).

320 We also simulated several point mutations at Asn348 in the hTfR1. As discussed above, the ala-
321 nine mutation at this site showed no significant difference in maximum applied force or AUC from
322 WT (Tables 4 and 5). In addition, neither the Asn348Lys nor the Asn348Trp mutation showed a sig-
323 nificant difference from WT. For both of these mutations, however, mean maximum applied force
324 and mean AUC was lower than for WT (See Table 2). On the other hand, there was a detectable
325 difference between Asn348Ala and Asn348Lys (Tables 4 and 5), with Asn348Lys being a weaker
326 binder. Moreover, Asn348Trp showed nearly identical results to Asn348Lys. The mutations to
327 large amino acids (Asn348Trp and Asn348Lys) produced nearly identical affinity changes, whereas
328 the mutations to amino acids not capable of hydrogen bonding (Asn348Ala and Asn348Trp) pro-
329 duced significantly different affinity changes (Table 3). To check the consistency of our results, we
330 hypothesized that the combination of Tyr211Ala and Asn348Trp, being chemically disconnected
331 in two different hydrogen-bonding networks, would lead to a synergistic loss-of-binding. As ex-
332 pected, the double mutant was the weakest binding mutant tested ($p < 10^{-6}$, Tables 4 and 5) in this
333 study. Further, according to maximum applied force (but not AUC), the combination of Tyr211Ala
334 and Asn348Trp also showed significantly weaker binding than Tyr211Ala by itself (Tables 4 and 5).
335 We suspect that the effect of Asn348Trp alone is near the limit of detection using our method. A
336 larger number of replicates would possibly have resolved affinity differences between Asn348Trp
337 and WT or other mutants more consistently.

338 Last, we further analyzed a single mutation in GP1, vArg111Ala. As mentioned previously, in

339 our simulations this mutant showed no significant change in either maximum applied force or AUC
340 (Tables 4 and 5), even though both quantities were, on average, lower than in WT (Table 2). This re-
341 sult was somewhat surprising, since Tyr211Ala, presumably disrupting the same hydrogen-bonding
342 network as vArg111Ala, displayed a significant reduction in affinity. To probe the interaction be-
343 tween position 111 in the GP1 and position 211 in the hTfR1 further, we also tested the double
344 mutant vArg111Ala/Tyr211Ala. This double mutant showed affinity indistinguishable from WT
345 and significantly higher than Tyr211Ala alone (Table 3). This result shows that the two sites do
346 indeed interact, and that replacing the hydrogen-bonding network at these sites with a hydrophobic
347 interaction could lead to comparable binding affinity.

348 **4 Discussion**

349 We have applied a method utilizing steering forces in all-atom molecular dynamics simulations
350 to evaluate the effects of mutations at the GP1/hTfR1 interface. We modeled mutations at sev-
351 eral sites in the GP1/hTfR1 interface, and verified that our computational protocol was sensitive
352 enough to distinguish point mutants in hTfR1. Further, we identified two test statistics, maximum
353 applied force and AUC, that can be used as proxies for binding affinity. Both of these statistics
354 correlate well with FEP, but offer the simplicity of not requiring a large commitment to planning
355 for the theoretical issues inherent to free energy methods. We systematically tested several point
356 mutations to understand their contribution to the binding interaction. In the case of Asn348Lys,
357 we have shown that the static structure provides little insight into why this mutation causes loss-
358 of-infectivity *in vivo*. While Asn348 appears to be involved in a hydrogen-bonding network in the
359 static structure, change in binding at that site may actually be caused by size and charge restriction.
360 We also found that a negatively polar residue at site 211 in hTfR1 seem critical for a tight binding
361 interaction. Any non-polar mutation at Tyr211 in hTfR1 is likely to completely halt viral entry and
362 dramatically decrease the chances of MACV infection.

363 Traditionally SMD has been either applied to compute equilibrium free energies via a non-
364 equilibrium approximation (Park et al. 2003; Park and Schulten 2004; Giorgino and Fabritiis 2011),
365 used to estimate protein stability through unfolding (Lu and Schulten 1999), or used to calculate the
366 absolute free energy of small molecule ligand binding (Dixit and Chipot 2001). Likewise, others

367 have used SMD to understand the process of binding and unbinding at a resolution unmatched by
368 experiment (Cuendet and Zoete 2011; Giorgino and Fabritiis 2011). Here, we have shown that
369 SMD can provide insight into the *relative* strength of protein–protein interactions. Via SMD, one
370 can separate mutations whose likely effect is altered binding affinity with simple statistics like
371 maximum force of separation. Thus, SMD may open avenues for subsequent experimental work in
372 some situations where FEP may be prohibitively difficult.

373 Our findings rationalize several effects observed in both infectivity data and rodent populations
374 (Radoshitsky et al. 2008; Choe et al. 2011). First, we found that some substitutions at positions
375 211 and 348 did affect the strength of receptor binding. However, the computational data suggest
376 that the reason and nature of the effects at these two sites are very different. At position 211,
377 mutations to non-polar residues cause a large change in binding. This is congruent with what is
378 known from viral entry data (Radoshitsky et al. 2008; Choe et al. 2011). By contrast, mutations
379 at position 348 need only be small to maintain WT binding. The ability to hydrogen bond appears
380 to be insignificant. This can be inferred from the fact that Tyr211Ala paired with large (Trp) and
381 positively charged (Lys) substitutions at position 348 results in a larger than expected synergistic
382 difference. That is, the double mutant Tyr211Ala/Asn348Trp caused a much larger decrease in
383 binding than we expected from either mutation individually. Third, the GP1 mutation vArg111Ala
384 causes a loss-of-infection during *in vitro* infectivity assays (Radoshitsky et al. 2011), yet it was
385 indistinguishable from the WT complex in our simulations. Although Tyr211Ala was the most
386 disruptive single mutant we tested, vArg111Ala in the GP1 was able to restore mean maximum
387 applied force to WT levels (Table 2), and to levels significantly higher than observed for Tyr211Ala
388 alone.

389 We would like to emphasize here that we cannot expect perfect agreement between our simula-
390 tions and the available experimental data, but the correspondence to a well established free energy
391 method bolsters our conclusions. While we have shown that our method can distinguish individual
392 point mutations, we do not know the limit of detection with our method. First, it is possible that
393 some mutants display measurable phenotypic effects in experiments yet appear identical in simula-
394 tion. More extensive sampling or refinement of the simulation protocol could help to differentiate
395 such mutants (see also next paragraph). Second, the SMD method is fundamentally limited by the
396 accuracy of our starting structure. Third, the available experimental data for the GP1/hTfR1 sys-

397 tem were generally obtained from entry assays or whole-cell binding assays rather than molecular
398 binding assays. A mutant may cause a phenotypic difference in infectivity without generating a
399 signal by our method. For example, entry could be lost in the experimental system because the
400 protein is grossly or partially misfolded. An additional analytical step with circular dichroism or an
401 analogous technique could clarify such large-scale folding differences. Further, since our simula-
402 tions start with a bound structure, any changes that may dramatically affect the rate of association
403 (different folds, trafficking issues, etc.) or relative orientation of the two proteins would be under-
404 estimated by our method.

405 There are a few additional challenges for investigating host-virus interactions via molecular
406 dynamics simulation. As with any atomistic simulation, there is going to be a fairly large noise-to-
407 signal ratio. To reduce noise, one could further customize each simulation, e.g. by determining the
408 optimal pulling speed. Furthermore, larger amounts of computational resources will have a direct
409 and powerful impact on the strength of any atomistic study (Jensen et al. 2012). Such resources
410 could come in the form of increased compute time, improved code, or customized hardware for
411 floating point operations (Shaw et al. 2011). With improved resources, we could investigate thou-
412 sands of individual permutations in the GP1/hTfR1 binding interface. In addition, with additional
413 compute time it would be possible to incorporate equilibrium sampling approaches (Buch et al.
414 2011) or use brute force equilibrium approaches (Giorgino et al. 2012) to improve resolution.

415 For future studies, although our approach offers the simplicity of not requiring prior knowledge
416 about a system of interest (other than a bound model), at this point SMD may not be the best approach
417 for many relative affinity calculations. To ensure one's results are independent of the dissociation
418 path one selects would require computing the work of separation for all likely paths. Such an
419 approach eventually requires using the Jarzynski inequality (Jarzynski 1997) to establish a lower
420 limit for binding energy and would quickly become computationally inefficient for evaluating a
421 large number of mutations in most systems. However, considering the strong correlation between
422 FEP and SMD in this system, it may not be important to ensure one's results are path independent
423 for relative affinity calculations, as long as the same path is used for all complexes.

424 More importantly, with no *a priori* knowledge of the appropriate number of equilibration sam-
425 ples, the best duration of equilibration, the appropriate number of pulling runs, or the best pulling
426 speed means the computational expense in our SMD protocol may not be commensurate with the

427 information provided. For example, another all atom approach that makes calculations via short
428 simulations of spatially restrained complexes has proven capable of generating relatively accurate
429 binding affinities with less compute time than is required from our steering strategy (Gumbart et al.
430 2013a,b). That being said, there is no reason to believe this SMD approach to mutagenic stud-
431 ies could not be optimized to reduce computational expense. Further analysis will be needed to
432 understand the lower limits of resources required for accurate predictions.

433 **5 Acknowledgements**

434 This work was carried out using high-performance computing resources provided by the High Per-
435 formance Computing Center (HPCC) at Texas Tech University at Lubbock (<http://www.hpcc.ttu.edu>)
436 and the Texas Advanced Computing Center (TACC) at The University of Texas at Austin (<http://www.tacc.utexas.edu>).
437 We would like to thank Bryan Sutton for opening access to the Hrothgar cluster and the reviewers
438 Ilan Samish and Matteo Masetti for their helpful comments on this work.

439 **References**

- 440 **Abraham J, Corbett K, Farzan M, Choe H, Harrison S. 2010.** Structural basis for receptor
441 recognition by new world hemorrhagic fever arenaviruses. *Nat. Struct. Mol. Bio.* **17**:438–444.
- 442 **Bajaj C, Chowdhury R, Siddahanavalli V. 2011.** F^2 Dock: Fast fourier protein-protein docking.
443 *IEEE Transactions on Computational Biology and Bioinformatics* **8**:45–58.
- 444 **Bakan A, Meireles L, Bahar I. 2011.** ProDy: Protein dynamics inferred from theory and experi-
445 ments. *Bioinformatics* **27**:1575–1577.
- 446 **Benjamini Y, Hochberg Y. 1995.** Controlling the false discovery rate: a practical and powerful
447 approach to multiple testing. *J. Royal Stat. Soc., Series B* **57**:289–300.
- 448 **Brooks B, Bruccoleri R, Olafson B, States D, Swaminathan S, Karplus M. 1983.** CHARMM:
449 A program for macromolecular energy, minimization, and dynamics calculations. *J. Comput.*
450 *Chem.* **4**:187–217.

451 **Buch I, Sadiq S, Fabritiis GD. 2011.** Optimized potential of mean force calculations for standard
452 binding free energies. *J. Chem. Theory Comput.* **7**:1765–1772.

453 **Charrel RN, de Lamballerie X. 2003.** Arenaviruses other than Lassa virus. *Antiviral Res.* **57**:89–
454 100.

455 **Chodera J, Mobley D, Shirts M, Dixon R, Branson K, Pande V. 2011.** Alchemical free energy
456 methods for drug discovery: progress and challenges. *Current Opinion in Structural Biology*
457 **21**:150–160.

458 **Choe H, Jemielity S, Abraham J, Radoshitzky S, Farzan M. 2011.** Transferrin receptor 1 in the
459 zoonosis and pathogenesis of new world hemorrhagic fever arenaviruses. *Current Opinion in*
460 *Microbiology* **12**:467–482.

461 **Cuendet M, Michielin O. 2008.** Protein-protein interaction investigated by steered molecular
462 dynamics: The TCR-PMHC complex. *Biophysical J.* **95**:3575–3590.

463 **Cuendet M, Zoete V. 2011.** How T-cell receptors interact with peptide-MHCs: A multiple steered
464 molecular dynamics study. *Proteins* **79**:3007–3024.

465 **Dixit S, Chipot C. 2001.** Can absolute free energies of association be estimated from molecular
466 mechanical simulations? The biotin-streptavidin system revisited. *J. Phys. Chem. A* **105**:9795–
467 9799.

468 **Gao J, Kuczera K, Tidor B, Karplus M. 1989.** Hidden thermodynamics of mutant proteins: A
469 molecular dynamics analysis. *Science* **244**:1069–1072.

470 **Gilson MK, Given JA, Bush BL, McCammon JA. 1997.** The statistical-thermodynamic basis for
471 computation of binding affinities: A critical review. *Biophys. J* **72**:11047–1069.

472 **Giorgino T, Buch I, Fabritiis GD. 2012.** Visualizing the induced binding of SH2-phosphopeptide.
473 *J. Chem. Theory Comput.* **8**:1171–1175.

474 **Giorgino T, Fabritiis GD. 2011.** A high-throughput steered molecular dynamics study on the free
475 energy profile of ion permeation through Gramicidin A. *J. Chem. Theory Comput.* **7**:1943–1950.

476 **Gront D, Kulp DW, Vernon RM, Strauss CEM, Baker D. 2011.** Generalized fragment picking
477 in Rosetta: Design, protocols and applications. *PLoS ONE* **6**.

478 **Gumbart J, Roux B, Chipot C. 2013a.** Standard binding free energies from computer simulations:
479 What is the best strategy? *J. Chem. Theory Comput.* **9**:794–802.

480 **Gumbart J, Schreiner E, Wilson D, Beckmann R, Schulten K. 2012.** Mechanisms of SecM-
481 mediated stalling in the ribosome. *Biophys. J.* **203**:331–341.

482 **Gumbart JC, Roux B, Chipot C. 2013b.** Efficient determination of protein-protein standard
483 binding free energies from first principles. *J. Chem. Theory Comput.* **9**:3780–3798.

484 **Humphrey W, Dalke A, Schulten K. 1996.** VMD - Visual Molecular Dynamics. *J. Molec.*
485 *Graphics* **14**:33–38.

486 **Hwang H, Vreven T, Janin J, Weng Z. 2010.** Protein-protein docking benchmark version 4.0.
487 *Proteins* **78**:3111–3114.

488 **Isralewitz B, Baudrya J, Gullingsruda J, Kosztinav D, Schulten K. 2001a.** Steered molecular
489 dynamics investigations of protein function. *J. Molec. Graphics* **19**:13–25.

490 **Isralewitz B, Gao M, Schulten K. 2001b.** Steered molecular dynamics and mechanical functions
491 of proteins. *Current Opinion in Structural Biology* **25**:225–230.

492 **Jarzynski C. 1997.** Equilibrium free-energy differences from nonequilibrium measurements: A
493 master-equation approach. *Physical Review E* **56**:5018–5035.

494 **Jensen M, Jogini V, Borhani D, Leffler A, Dror R, Shaw D. 2012.** Mechanism of voltage gating
495 in potassium channels. *Science* **336**:229–233.

496 **Kortemme T, Kim DE, Baker D. 2004.** Computational alanine scanning of protein-protein inter-
497 faces. *Sci. STKE* **2004**:12.

498 **Liu P, Dehez F, Cai W, Chipot C. 2012.** A toolkit for the analysis of free-energy perturbation
499 calculations. *J. Chem. Theor. Comput.* **8**:2606–2616.

500 **Lu H, Schulten K. 1999.** Steered molecular dynamics simulations of force-induced protein domain
501 unfolding. *Protein Struct. Funct. Genet.* **35**:453–463.

502 **Lu N, Kofke DA, Woolf TB. 2004.** Improving the efficiency and reliability of free energy pertur-
503 bation calculations using overlap sampling methods. *J. Comput. Chem.* **25**:28–39.

504 **Miño G, Baez M, Gutierrez G. 2013.** Effect of mutation at the interface of Trp-repressor dimeric
505 protein: a steered molecular dynamics simulation. *Eur. Biophys. J.* **42**:683–690.

506 **Michaud-Agrawal N, Denning E, Woolf T, Beckstein O. 2011.** MDAAnalysis: A toolkit for the
507 analysis of molecular dynamics simulations. *J. Comput. Chem.* **32**:2319–2327.

508 **Park S, Khalili-Araghi F, Tajkhorshid E, Schulten K. 2003.** Free energy calculation from steered
509 molecular dynamics simulations using Jarzynski’s equality. *J. Chem. Phys.* **119**:3559–3567.

510 **Park S, Schulten K. 2004.** Calculating potentials of mean force from steered molecular dynamics
511 simulations. *J. Chem. Phys.* **120**:5946–5961.

512 **Pearlman DA. 1989.** A comparison of alternative approaches to free energy calculations. *J. Phys.*
513 *Chem.* **98**:1487–1493.

514 **Phillips J, Braun R, Wang W, Gumbart J, Tajkhorshid E, Villa E, Chipot C, Skeel R, Kale L,**
515 **Schulten K. 2005.** Scalable molecular dynamics with NAMD. *J. Comput. Chem.* **26**:1781–1802.

516 **Radoshitsky S, Kuhn J, Spiropoulou C, Albarino C, Nguyen D, Salazar-Bravo J, Dorfman**
517 **T, Lee A, Wang E, Ross S, Choe H, Farzan M. 2008.** Receptor determinants of zoonotic
518 transmission of new world hemorrhagic fever arenaviruses. *Proc. Natl. Acad. Sci.* **19**:2664–
519 2669.

520 **Radoshitsky S, Longobardi L, Kuhn J, Retterer C, Clester J, K Kota JC, Bavari S. 2011.**
521 Machupo virus glycoprotein determinants for human transferrin receptor 1 binding and cell entry.
522 *PLoS ONE* **6**.

523 **Schrödinger. 2010.** The PyMOL molecular graphics system, version 1.3r1. Schrödinger, LLC.

524 **Shaw D, Dror R, Salmon J, Grossman J, Mackenzie K, Bank J, Young C, Deneroff M, Batson**
525 **B, Bowers K, Chow E, Eastwood M, Ierardi D, Klepeis J, Kuskin J, Larson R, Lindorff-**
526 **Larsen K, Maragakis P, Moraes M, Piana S, Shan Y, Towles B. 2011.** Millisecond-scale
527 molecular dynamics simulations on anton. *Proceedings of the Conference on High Performance*
528 *Computing, Networking, Storage and Analysis SC09*:39.

529 **Vreven T, Hwang H, Pierce B, Weng Z. 2012.** Prediction of protein-protein binding free energies.
530 *Protein Science* **21**:396–404.

531 **Vreven T, Hwang H, Weng Z. 2011.** Integrating atom-based and residue-based scoring functions
532 for protein-protein docking. *Protein Science* **20**:1576–1586.

533 **Wang J, Deng Y, Roux B. 2006.** Absolute binding free energy calculations using molecular dy-
534 namics simulations with restraining potentials. *Biophys. J.* **91**:2798–2814.

535 **Wickham H. 2009.** *ggplot2: Elegant graphics for data analysis.* Springer New York. URL
536 <http://had.co.nz/ggplot2/book>.

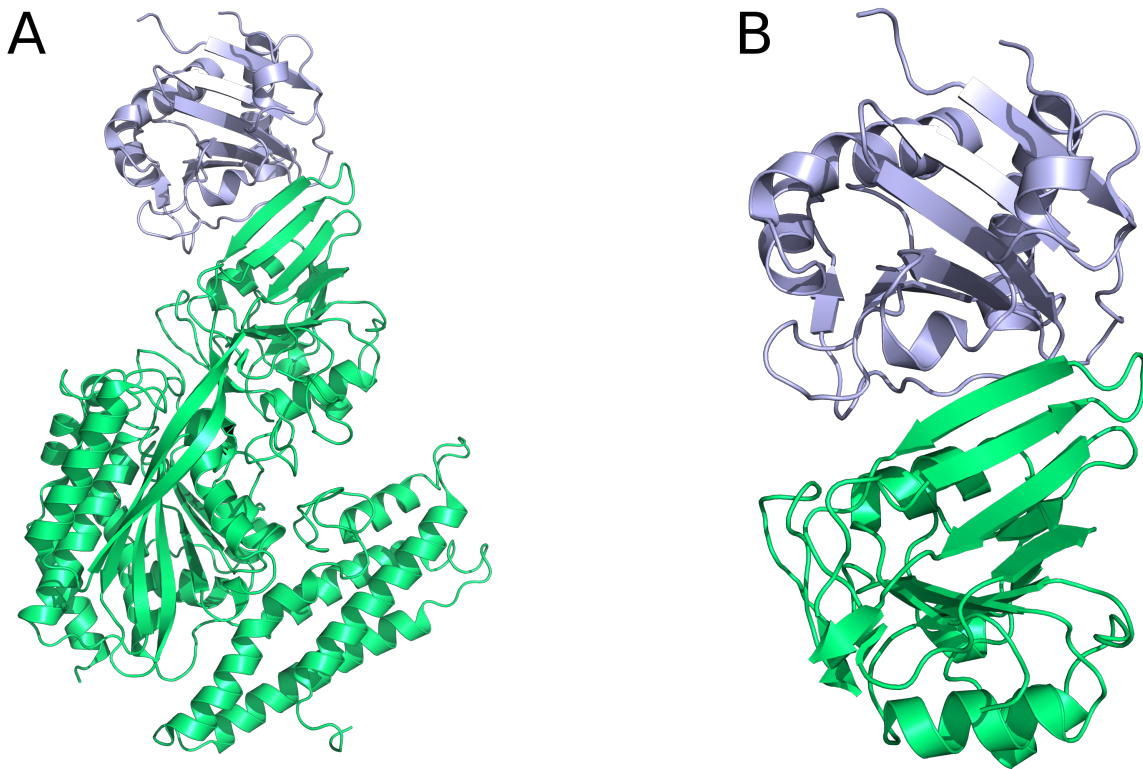


Figure 1: The GP1/hTfR1 complex. GP1 is shown in blue and hTfR1 is shown in green. (A) The full, de-glycosylated GP1/hTfR1 co-crystal structure. (B) The reduced structure used in SMD simulations.

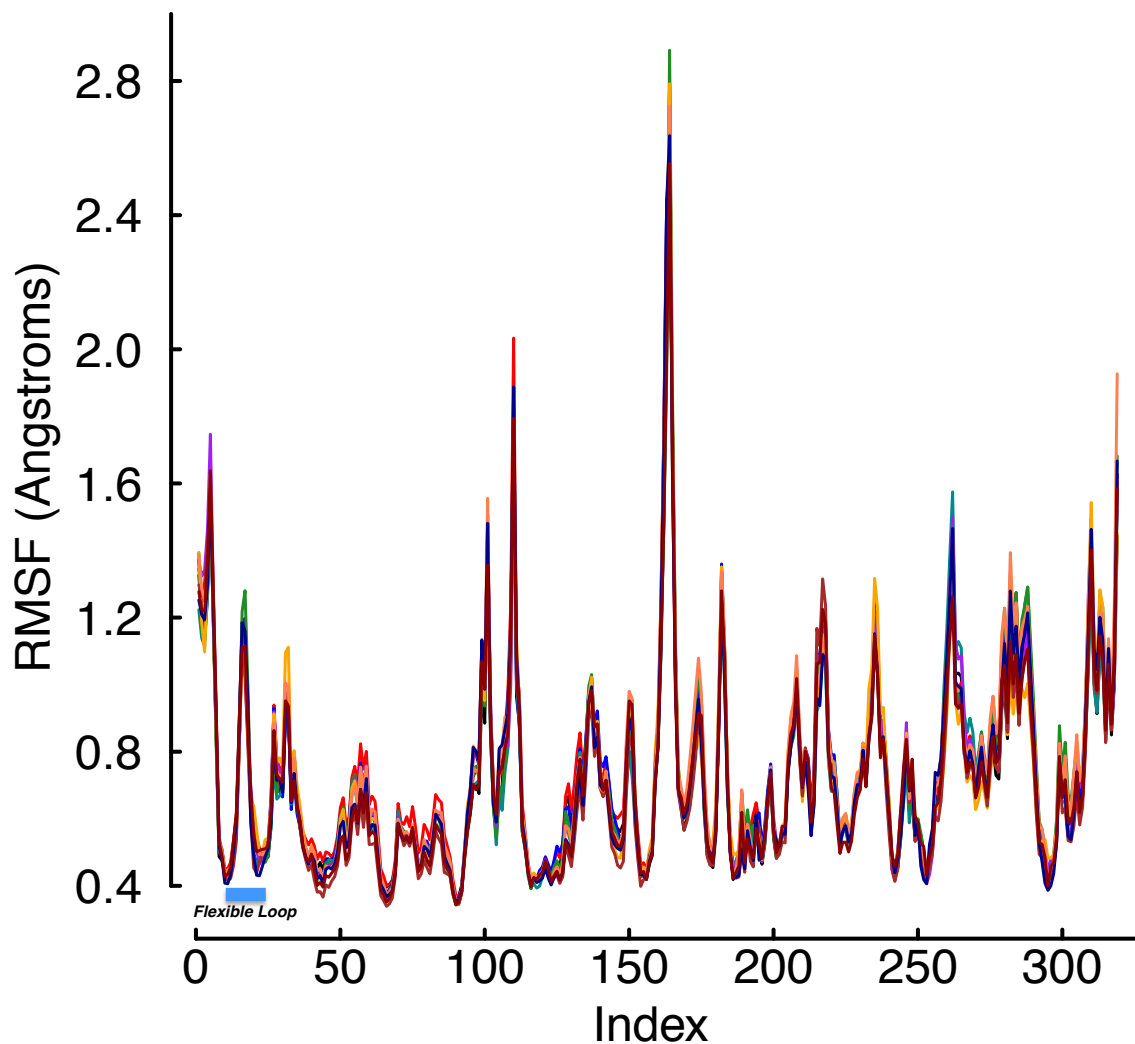


Figure 2: RMSF values during equilibration. The RMSF values for every site in the bound complex computed during the equilibration phase of the protocol. Each color represents the average over 20 trajectories of a single mutant. Indices 17-25 are the hTfR flexible loop. The plot shows the flexibility of each site is essentially independent of mutation, and two sites (indices 17 and 18) above 0.72 Å are a part of the flexible loop in the free receptor. However, these two residues are not actually found in the protein–protein interface, but rather are almost completely solvent exposed with the virus bound.

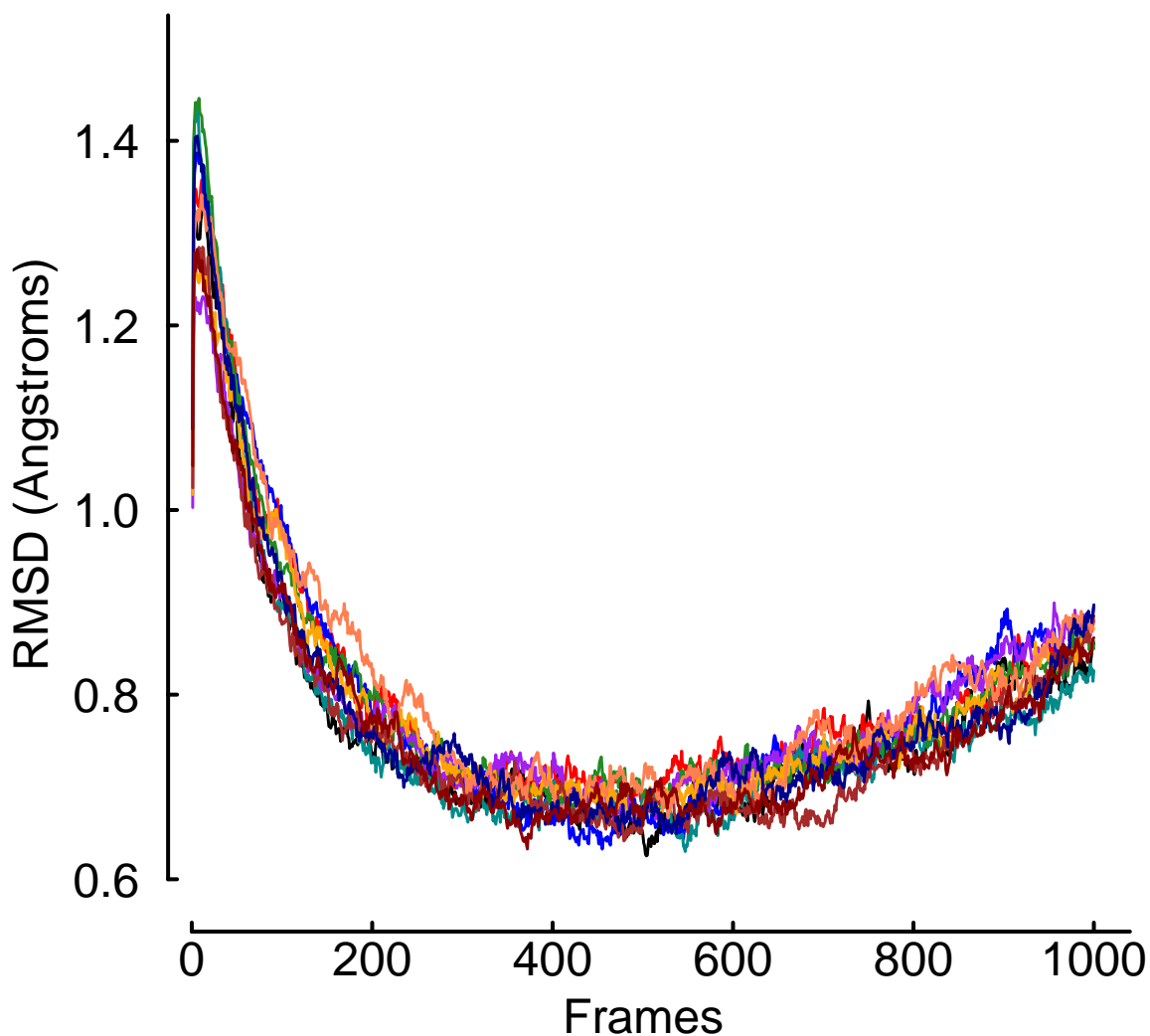


Figure 3: RMSD values during equilibration. The RMSD values over the time of the trajectory computed during the equilibration phase of the protocol. Each color represents the average over 20 trajectories of a single mutant. The plot shows none of the mutants causes immediate unbinding of the protein–protein complex. In addition, the universal upward trend near the end of the equilibration trajectories may indicate the crystal is more tightly packed than would normally occur in solution.

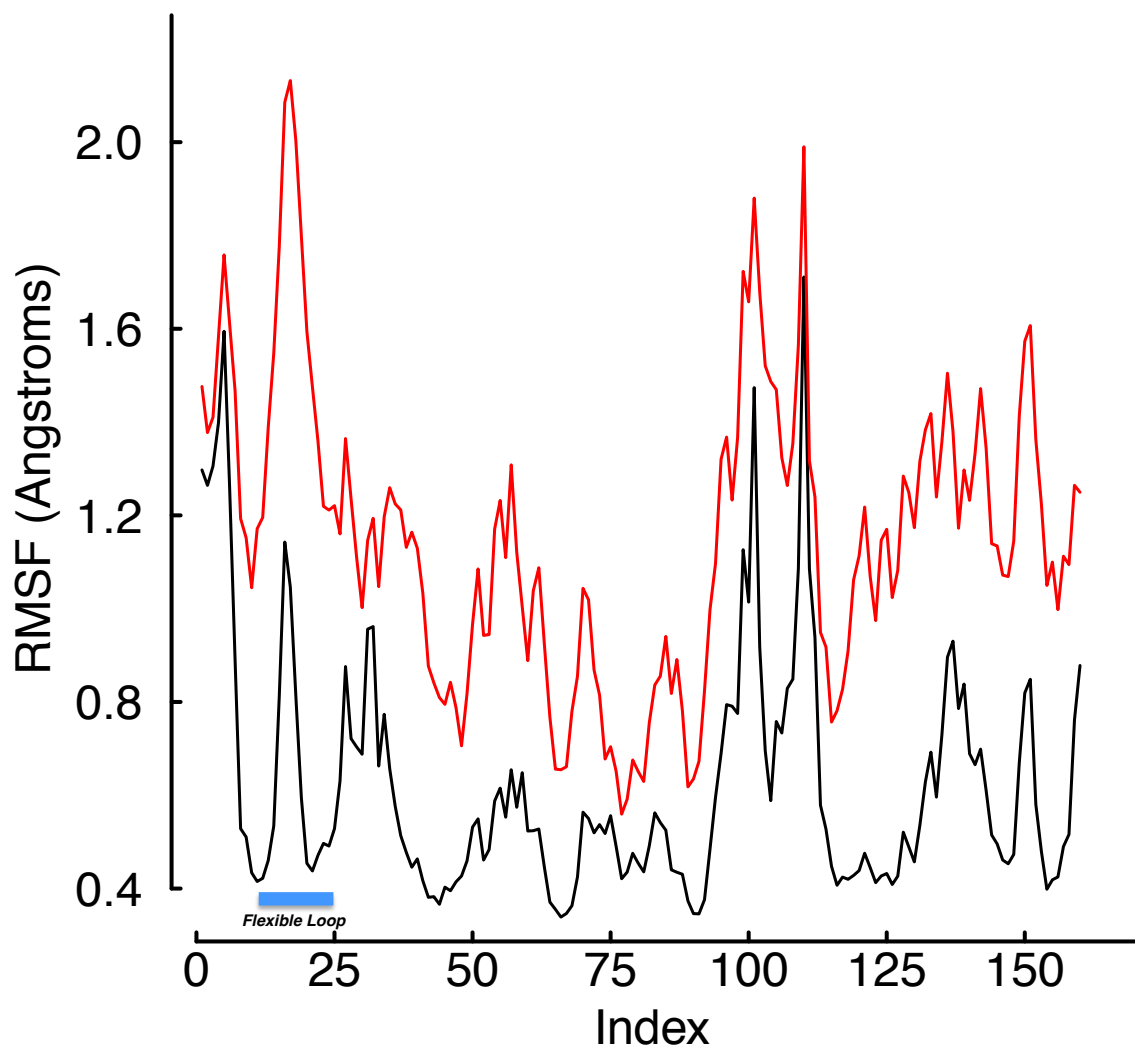


Figure 4: RMSF values of WT hTfR in equilibration and SMD. The RMSF values for every site in the WT receptor were computed during the equilibration phase and during final 50 frames of the SMD trajectories. The black line was computed over equilibration and the red line during SMD. The plot shows the solution mobility of the hTfR flexible loop increases more than the average during the unbinding process.

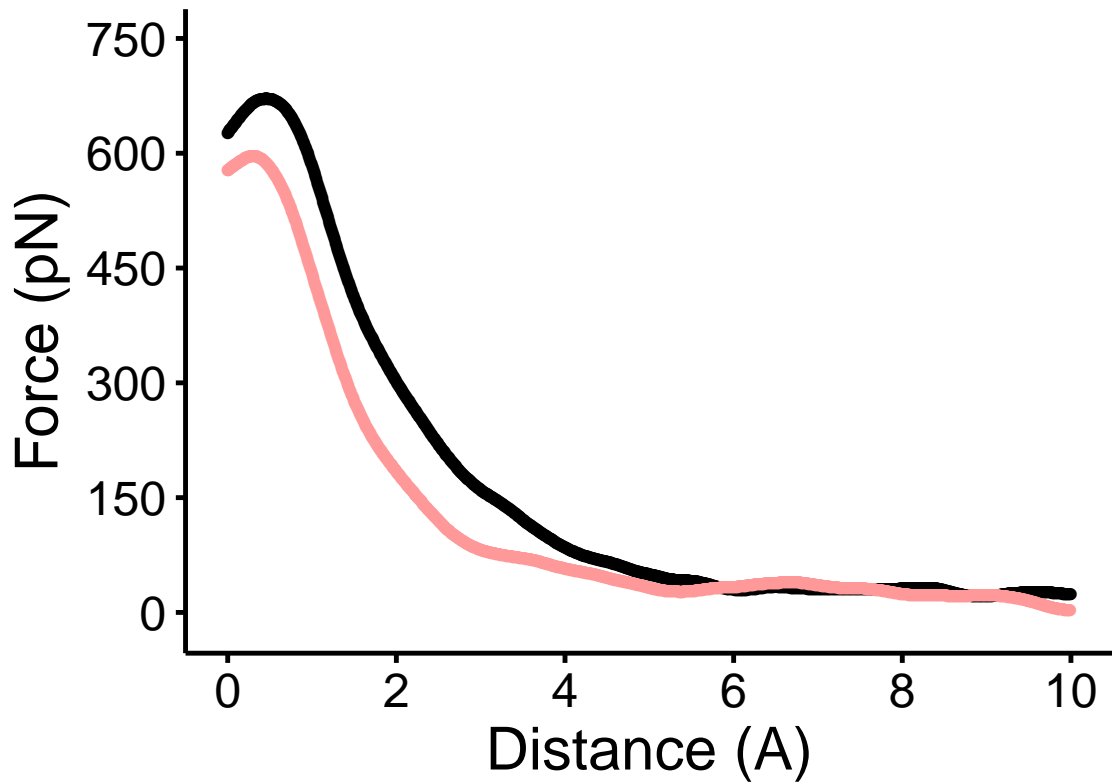


Figure 5: Force versus distance curve of WT and the Y211A mutant. The average force curve for 50 replicates of the WT complex is shown in black, and the average of 50 replicates of the Y211A mutant is shown in red. There is a large difference in both maximum applied force and AUC between the two complexes.

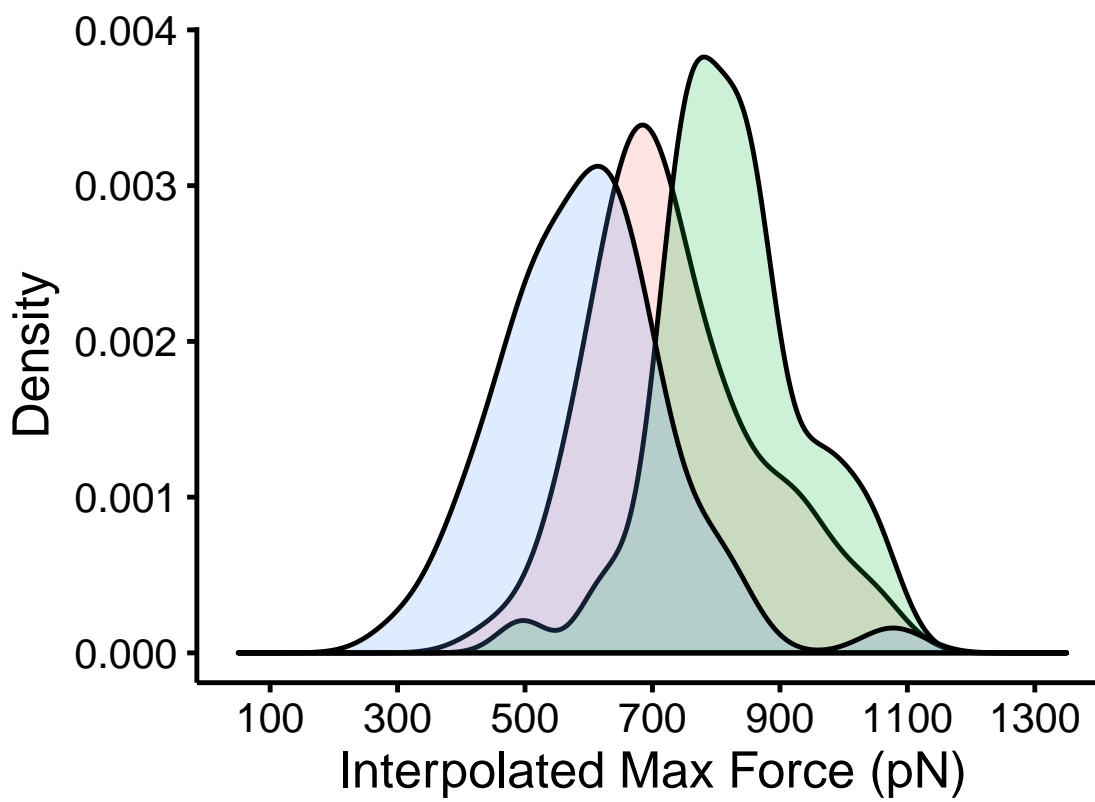


Figure 6: Distribution of interpolated maximum force for three different GP1/hTfR1 complexes. The WT GP1-hTfR1 complex in the middle is flanked by the tighter binding mutant Y211D on the right and the weaker binding double mutant N348W/Y211A on the left. The large non-overlapping areas indicate a large and statistically significant difference in these three complexes.

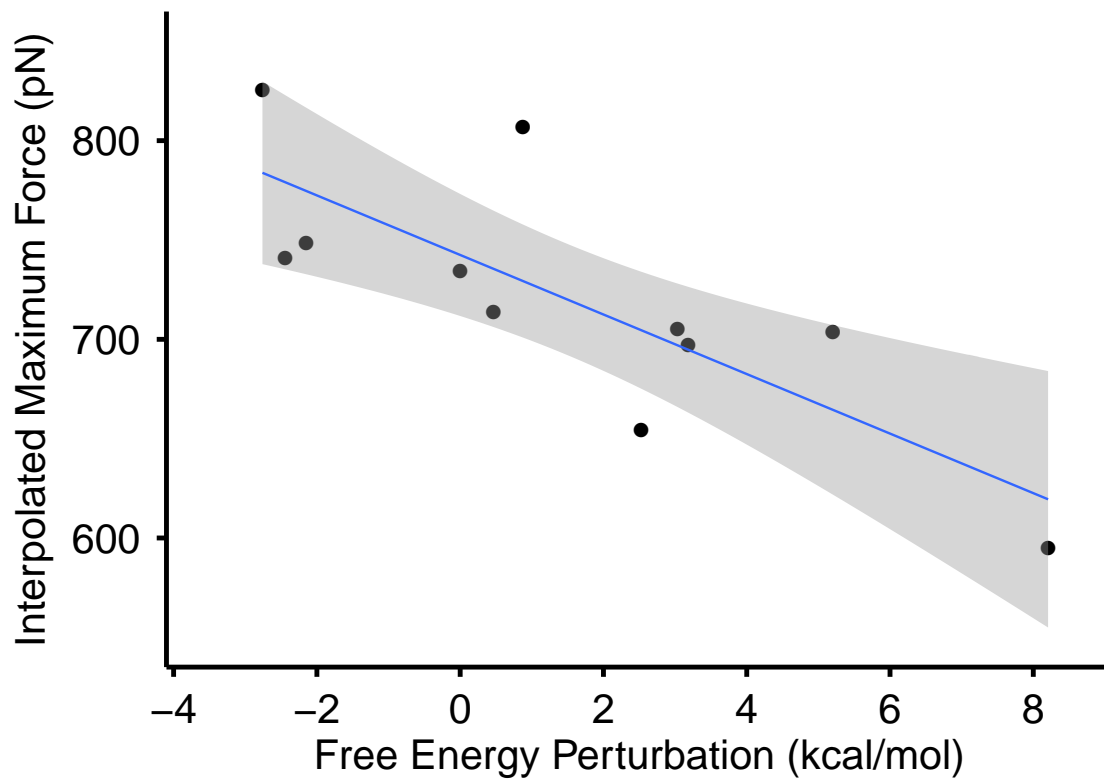


Figure 7: Max force versus free energy perturbation. Scatter plot of maximum force in SMD versus the relative free energy difference calculated by FEP for all 10 mutants tested plus the WT complex. The WT complex for FEP was simply set to 0.0. The correlation between the two is $r = -0.795$ with $p = 0.0034$.

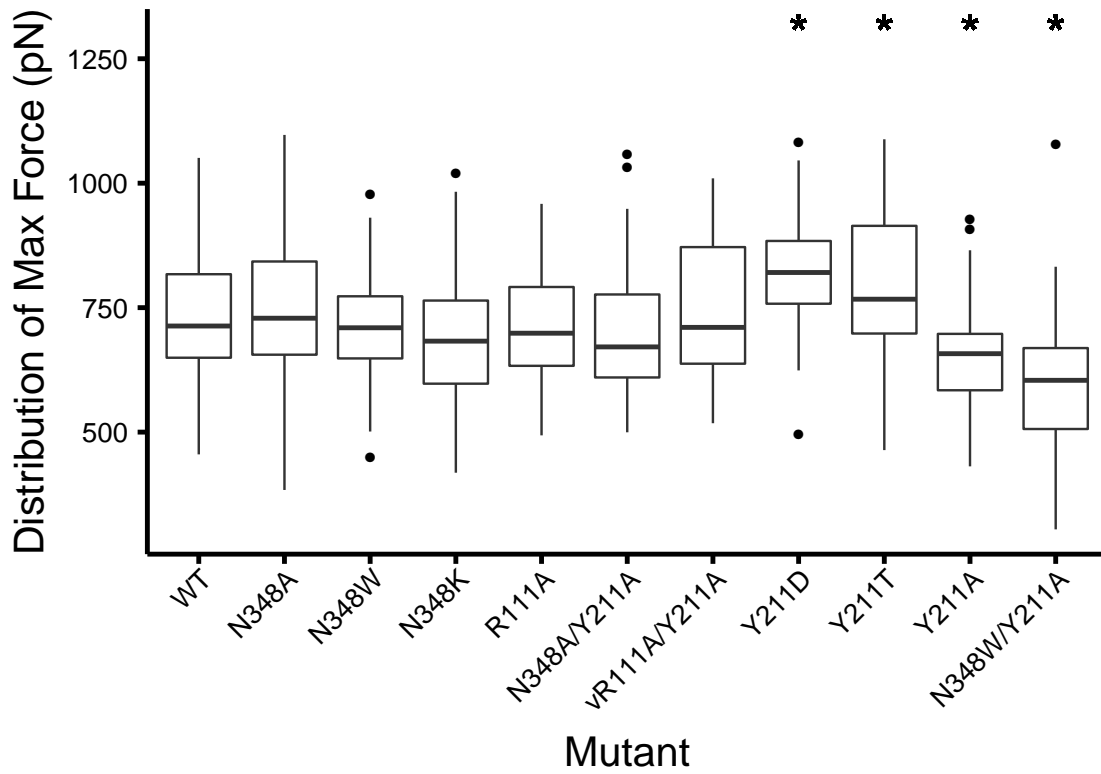


Figure 8: Distribution of interpolated maximum force for all bound complexes tested. Stars above the boxplots indicate a statistically significant difference in mean maximum force relative to the WT complex.

Table 1: Summary of prior information available for each mutation tested. Observed *in vivo* refers to mutations that have been observed in rodent populations. Phenotype *in vitro* refers to the observed phenotype in *in vitro* viral entry assays.

Mutation	Observed <i>in vivo</i>	Phenotype <i>in vitro</i>
WT	Yes	Normal Entry
N348A	No	-
N348K	Yes	Diminished Entry
N348W	No	-
vR111A	No	Diminished Entry
N348A/Y211A	No	-
vR111A/Y211A	No	-
Y211D	Yes	No Expression
Y211T	No	Diminished Entry
Y211A	No	No Expression
N348W/Y211A	No	-

Table 2: Summary statistics for each mutation tested. μ_{MAF} is the mean in piconewtons and σ_{MAF} is the standard deviation of maximum applied force over all simulations. μ_{AUC} is the mean and σ_{AUC} is the standard deviation of AUC over all simulations. ΔG is the free energy difference in kcal/mol calculated via FEP by the dual topology paradigm.

Mutation	μ_{MAF} (pN)	σ_{MAF}	μ_{AUC}	σ_{AUC}	ΔG (kcal/mol)
WT	734.4856	131.6513	145460.4	60232.26	0.000
N348A	748.5217	137.4864	133913.9	51078.64	-2.149
N348K	705.0707	108.5079	141084.4	54450.28	+3.184
N348W	697.3642	132.6436	136886.0	53796.44	+3.033
vR111A	713.8081	106.7374	136103.2	52070.85	+0.466
N348A/Y211A	703.7027	128.5866	113464.2	57451.62	+5.203
vR111A/Y211A	741.0642	131.6287	130070.6	47665.56	-2.440
Y211D	825.2586	115.4343	158878.7	63039.08	+2.760
Y211T	806.8593	136.5648	167110.7	78849.29	+0.875
Y211A	654.1138	108.5343	108090.0	43661.09	+2.526
N348W/Y211A	594.9044	134.8233	108984.2	45451.00	+8.206

Table 3: Pairwise differences (row variable minus column variable) in mean maximum applied force. Bolded values are statistically significant at $p < 0.05$.

	WT	N348A	N348W	N348K	vR111A	N348A/Y211A	vR111A/Y211A	Y211D	Y211T	Y211A
N348A	+14.036									
N348W	-29.414	-43.451								
N348K	-37.121	-51.157	-7.7060							
vR111A	-20.677	-34.713	+8.7370	+16.443						
N348A/Y211A	-30.782	-44.819	-1.3670	+6.3380	-10.105					
vR111A/Y211A	+6.5790	-7.4570	+35.993	+43.700	+27.256	+37.361				
Y211D	+90.772	+76.736	+120.19	+127.89	+111.45	+121.56	+84.194			
Y211T	+72.373	+58.337	+101.79	+109.50	+93.051	+103.16	+65.795	-18.399		
Y211A	-80.371	-94.407	-50.956	-43.250	-59.694	-49.588	-86.950	-171.14	-152.75	
N348W/Y211A	-139.58	-153.62	-110.17	+102.46	-118.903	-108.80	+146.16	+230.35	-211.95	-59.209

Table 4: Pairwise difference p -values for maximum applied force. Bolded values are statistically significant at $p < 0.05$.

	WT	N348A	N348W	N348K	vR111A	N348A/Y211A	vR111A/Y211A	Y211D	Y211T	Y211A
N348A	0.60									
N348W	0.31	0.077								
N348K	0.20	0.038	0.81							
vR111A	0.51	0.16	0.79	0.60						
N348A/Y211A	0.29	0.07	0.95	0.81	0.77					
vR111A/Y211A	0.82	0.79	0.21	0.13	0.35	0.20				
Y211D	0.00093	0.0012	1.4×10^{-5}	5.0×10^{-6}	5.6×10^{-5}	1.2×10^{-5}	0.0022			
Y211T	0.01	0.018	0.00022	8.7×10^{-5}	0.0008	0.0002	0.021	0.56		
Y211A	0.0034	7.2×10^{-5}	0.074	0.13	0.035	0.079	0.0016	4.2×10^{-10}	4.2×10^{-8}	
N348W/Y211A	3.9×10^{-7}	1.1×10^{-10}	6.5×10^{-5}	0.00021	1.6×10^{-5}	7.2×10^{-5}	1.3×10^{-7}	2×10^{-16}	2.0×10^{-14}	0.036

Table 5: Pairwise difference p -values for interpolated AUC. Bolded values are statistically significant at $p < 0.05$.

	WT	N348A	N348W	N348K	vR111A	N348A/Y211A	vR111A/Y211A	Y211D	Y211T	Y211A
N348A	0.33									
N348W	0.76	0.59								
N348K	0.59	0.80	0.76							
vR111A	0.55	0.85	0.76	0.94						
N348A/Y211A	0.017	0.07	0.031	0.076	0.08					
vR111A/Y211A	0.26	0.76	0.46	0.68	0.72	0.22				
Y211D	0.33	0.029	0.18	0.09	0.08	0.00046	0.029			
Y211T	0.09	0.0056	0.046	0.027	0.023	4.1×10^{-5}	0.006	0.59		
Y211A	0.0056	0.027	0.016	0.029	0.031	0.75	0.09	8.2×10^{-5}	8.5×10^{-6}	
N348W/Y211A	0.006	0.029	0.017	0.032	0.034	0.76	0.1	9.4×10^{-5}	8.5×10^{-6}	0.94